

Phoretic swimming with bulk absorption

Rodolfo Brandão

*Department of Mechanical and Aerospace Engineering,
Princeton University, Princeton, New Jersey 08544, USA*

David Saintillan

*Department of Mechanical and Aerospace Engineering,
University of California San Diego, La Jolla, California 92093, USA*

Ehud Yariv

Department of Mathematics, Technion — Israel Institute of Technology, Haifa 32000, Israel

(Dated: October 10, 2023)

Abstract

We consider phoretic self-propulsion of a chemically active colloid where solute is consumed at both the colloid boundary and within the bulk solution. Assuming first-order kinetics, the dimensionless transport problem is governed by the surface Damköhler number \mathcal{S} and the bulk Damköhler number \mathcal{B} . The dimensionless colloid velocity U , normalized by a self-phoretic scale, is a nonlinear function of these two parameters. We identify two scenarios where these numbers are linked. When the controlling physical parameter is colloid size, \mathcal{S} is proportional to $\mathcal{B}^{1/2}$; when the controlling parameter is solute diffusivity, \mathcal{S} is proportional to \mathcal{B} . In the limit of small Damköhler numbers, U adopts the same asymptotic limit in both scenarios, proportional to \mathcal{S} . In the limit of large Damköhler numbers, the deviations of solute concentration from the equilibrium value are restricted to a narrow layer about the active portion of the colloid boundary. The asymptotic predictions of the associated boundary-layer problem are corroborated by an eigenfunction solution of the exact problem. The boundary-layer structure breaks down near the transition between the active and inactive portions of the boundary. The transport problem in that local region partially resembles the classical Sommerfeld problem of wave diffraction from an edge.

I. INTRODUCTION

The remarkable propulsion exhibited by chemically active particles in liquid solutions, known as self-diffusiophoresis, has garnered significant attention following experimental breakthroughs in catalytic swimmers [1]. The fundamental mechanism underpinning phoretic self-propulsion involves two key components: solute production or consumption at the particle boundary, coupled with short-range interactions between the solute molecules and that boundary. Golestanian *et al.* [2] introduced the first macroscale model to describe self-diffusiophoresis under Stokes flow conditions, accounting for diffusive solute transport. In that mode, chemical reactions at the particle boundary are represented through a prescribed solute flux distribution, while mechanical interactions with solute molecules are captured through a diffusio-osmotic slip velocity — proportional to the tangential solute gradient at the outer edge of the interaction layer [3]. In the absence of solute advection, the linearity of the governing equations and boundary conditions implies that an asymmetry in the particle shape or physicochemical properties is required for self-propulsion: in typical experiments involving spherical colloids, this asymmetry is achieved by coating half of a particle with a catalyst.

A more sophisticated model of surface reactions, which better describes experimental systems, involve first-order chemical kinetics [4]. The associated boundary condition imposes a linear relation between the solute flux and local concentration, whose characteristic ratio defines the surface Dahmköhler number (hereafter denoted by \mathcal{S}). For slow reaction rates ($\mathcal{S} \rightarrow 0$), the imposed flux model is recovered. Accounting for finite Dahmköhler number has proven to be essential for capturing the dependence of the propulsion speed on particle size, as observed in experiments [4].

Of interest to us in this work is the case where the excess solute gets consumed in the bulk liquid surrounding the particle, for instance as a result of chemical degradation or bulk reaction with another solute. In that case, the strength of consumption is characterized by a bulk Dahmköhler number, hereafter denoted by \mathcal{B} , defined as the ratio of the reactive to diffusive consumption rates. Solute bulk absorption has already been studied using both numerical simulations [5] as well as weakly nonlinear analyses near the threshold for spontaneous motion [6]. In certain ill-posed (e.g. steady self-phoresis in two dimensions [7, 8]) and singular (e.g. spontaneous particle motion in channels [9]) problems, even a weak bulk

reaction may have significant effect.

Here, we analyze the steady motion of a spherical self-phoretic particle. The paper is organized as follows. We formulate the problem in Sec. II and present the dimensionless governing equations in Sec. III. An exact solution based upon an eigenfunction expansion is derived in Sec. IV. The linkage between the two Damköhler numbers is discussed in Sec. V, where we also consider the case of small \mathcal{S} and \mathcal{B} . The limit of large Damköhler numbers is addressed in Sec. VI. The associated boundary-layer analysis breaks down near the junction between the active and inactive portions of the particle boundary. We analyze the structure of this transition region in Sec. VII. Illustrative examples are presented in Sec. VIII. We conclude in Sec. IX.

II. PROBLEM FORMULATION

A chemically active spherical particle (radius a) is freely suspended in an unbounded solution (solute diffusivity D). The equilibrium solute concentration, at large distances from the particle, is denoted by c_∞ . Solute transfer at the particle boundary is modeled using a first-order chemical reaction [4],

$$\text{solute absorption (per unit area)} = k \times \text{local solute concentration}, \quad (2.1)$$

where the (positive) rate constant k generally varies along the boundary. In addition, we assume [5, 10] that solute is consumed in the bulk in proportion to the excess concentration — the deviation of its concentration from the equilibrium value,

$$\text{solute consumption (per unit volume)} = k_b \times \{\text{local solute concentration} - c_\infty\}. \quad (2.2)$$

The (positive) bulk rate k_b is assumed uniform.

Following the prevailing practice [4, 11], we restrict the subsequent analysis to situations where k is symmetric about an axis passing through the particle center; self-propulsion accordingly takes place in the form of rigid translation in a direction parallel to that axis. Our goal is the associated speed.

Defining \bar{k} as a characteristic norm of k , relation (2.1) leads to the definition of the Damköhler number,

$$\mathcal{S} = \frac{a\bar{k}}{D}, \quad (2.3)$$

representing the ratio of reactive ($\bar{k}c_\infty$) to diffusive (Dc_∞/a) solute flux densities. The problem is also affected by the bulk Damköhler number,

$$\mathcal{B} = \frac{a^2 k_b}{D}, \quad (2.4)$$

representing the ratio of reactive ($k_b c_\infty$) to diffusive (Dc_∞/a^2) consumption rates.

We employ a macroscale description, where the short-range interaction between the solute molecules and the particle is manifested by diffusio-osmotic slip [3],

$$\text{slip velocity} = b \times \text{surface gradient of solute concentration}. \quad (2.5)$$

We assume that b is uniform. Note that b is a signed quantity, positive for repulsive interactions and negative for attractive ones. The velocity scale associated with (2.5) is $\mathcal{U} = bc_\infty/a$.

We adopt a co-moving reference frame with the origin at the particle center. In that frame we utilize the spherical coordinates (ar, θ, ϕ) defined such that the axis $\theta = 0, \pi$ is aligned along the symmetry diameter of the particle and $r = 1$ is the particle boundary, see Fig. 1. The specified axially-symmetric activity is then represented by the function $k(\theta)$.

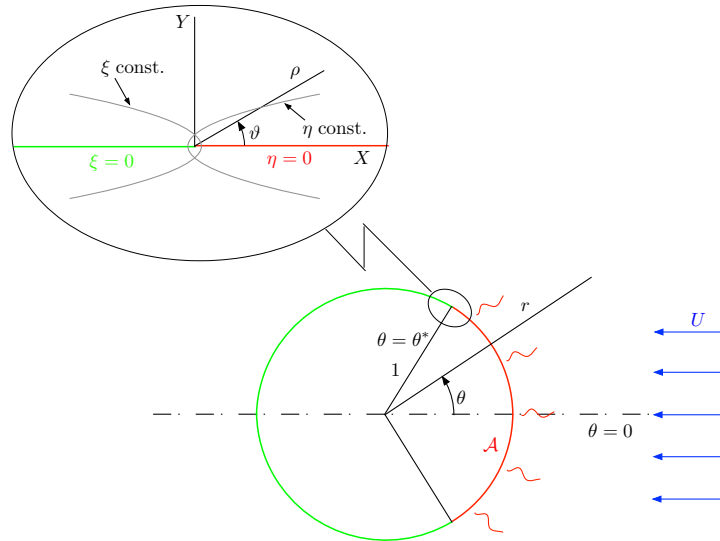


FIG. 1. Schematic showing the particle geometry and coordinates. The zoomed region (rotated) describes the transition-region coordinates.

Consistently with the macroscale description, the particle acquires the rectilinear velocity required to keep it force-free. Due to the axial symmetry, the particle velocity relative to

the otherwise quiescent liquid must be parallel to the symmetry axis, say $U^*\hat{\mathbf{i}}$ ($\hat{\mathbf{i}}$ being a unit vector in the direction $\theta = 0$). Our goal is the calculation of U^* .

III. DIMENSIONLESS DESCRIPTION

In what follows we consider the coupled transport–flow problem governing the excess solute concentration c , normalized by c_∞ , and fluid velocity \mathbf{u} , normalized by \mathcal{U} . Given the presumed axial symmetry, c is a function of r and θ . In the particle-fixed reference frame, the velocity of the particle is manifested as the uniform streaming $-U\hat{\mathbf{i}}$ at infinity, where $U = U^*/\mathcal{U}$.

The dimensionless solute transport problem is governed by: (i) the diffusion–reaction equation,

$$\nabla^2 c = \mathcal{B}c, \quad (3.1)$$

wherein

$$\nabla^2 = \frac{\partial}{\partial r^2} + \frac{2}{r} \frac{\partial}{\partial r} + \frac{1}{r^2 \sin^2 \theta} \frac{\partial^2}{\partial \theta^2} \quad (3.2)$$

is the pertinent dimensionless Laplacian; (ii) the kinetic condition at the particle boundary,

$$\frac{\partial c}{\partial r} = \mathcal{S}(1+c)f(\theta) \quad \text{at } r = 1, \quad (3.3)$$

where $f(\theta) = k(\theta)/\bar{k}$ is the dimensionless distribution of rate constant; and (iii) the approach to equilibrium at large distances,

$$c \rightarrow 0 \quad \text{as } r \rightarrow \infty. \quad (3.4)$$

Note that condition (3.3) is meaningful only with solute consumption, $f \geq 0$. The preceding problem provides c as a function of the governing parameters \mathcal{S} and \mathcal{B} , as well as $f(\theta)$. Once solved, we can consider the flow, governed by: (i) the continuity and Stokes equations [the former tacitly employed in (3.1)]; (ii) the diffusio-osmotic slip [cf. (2.5)]

$$\mathbf{u} = \hat{\mathbf{e}}_\theta \frac{\partial c}{\partial \theta} \quad \text{at } r = 1; \quad (3.5)$$

(iii) the far-field approach to a uniform stream (see Fig. 1),

$$\mathbf{u} \rightarrow -U\hat{\mathbf{i}} \quad \text{as } r \rightarrow \infty; \quad (3.6)$$

and (iv) the requirement that the particle is force-free. In fact, the detailed calculation of the flow field is not required, as use of the reciprocal theorem [12] provides U as the quadrature

$$U = \frac{1}{2} \int_0^\pi \left. \frac{\partial c}{\partial \theta} \right|_{r=1} \sin^2 \theta d\theta, \quad (3.7)$$

or, following integration by parts,

$$U = - \int_0^\pi c|_{r=1} \sin \theta \cos \theta d\theta. \quad (3.8)$$

In what follows, it may be convenient to employ $\mu = \cos \theta$ instead of θ . Writing $f(\theta) = F(\mu)$, it is natural to represent F as a series of surface harmonics,

$$F(\mu) = \sum_{m=0}^{\infty} F_m P_m(\mu) \quad (3.9)$$

wherein P_m are the Legendre polynomials of degree m . Using the orthogonality of these polynomials,

$$\int_{-1}^1 P_m(\mu) P_n(\mu) d\mu = \frac{2}{2m+1} \delta_{mn}, \quad (3.10)$$

we obtain

$$F_m = \frac{2m+1}{2} \int_{-1}^1 F(\mu) P_m(\mu) d\mu. \quad (3.11)$$

When using μ , (3.8) simplifies to

$$U = - \int_{-1}^1 \mu c|_{r=1} d\mu. \quad (3.12)$$

IV. EXACT SOLUTION

Using the eigenfunctions of the modified Helmholtz equation, we find that the most general axisymmetric solution of (3.1)–(3.2) and (3.4) is

$$c = \sum_{n=0}^{\infty} A_n r^{-1/2} K_{n+1/2}(\mathcal{B}^{1/2} r) P_n(\cos \theta). \quad (4.1)$$

Here K_ν are the modified Bessel functions of the second kind with degree ν . Substitution of (3.9) and (4.1) into condition (3.3) yields

$$\begin{aligned} \sum_{n=0}^{\infty} A_n \left[K'_{n+1/2}(\mathcal{B}^{1/2}) - \frac{1}{2} K_{n+1/2}(\mathcal{B}^{1/2}) \right] P_n(\mu) \\ = \mathcal{S} \left[1 + \sum_{n=0}^{\infty} A_n K_{n+1/2}(\mathcal{B}^{1/2}) P_n(\mu) \right] \sum_{m=0}^{\infty} F_m P_m(\mu), \quad (4.2) \end{aligned}$$

where the prime denote differentiation with respect to the argument. Projection of (4.2) upon $P_m(\mu)$ ($m = 0, 1, 2, \dots$) yields an infinite linear system governing the coefficients $\{A_n\}_{n=0}^\infty$. Using controlled truncation, this system may be solved in principle for any values of \mathcal{B} and \mathcal{S} and a given activity distribution $f(\theta)$. Once solved, substitution into (3.12) yields, upon making use of the orthogonality relations (3.10),

$$U = -\frac{2}{3}A_1K_{3/2}(\mathcal{B}^{1/2}). \quad (4.3)$$

Prior to illustrating the exact solution for a specific activity distribution, it is desirable to supplement it by asymptotic approximations.

V. LINKED DAMKÖHLER NUMBERS

Considering the manner by which the Damköhler numbers (2.3)–(2.4) depend upon the dimensional quantities in the problem, there are two natural scenarios where these two numbers are linked. The first scenario,

$$\mathcal{S} \propto \sqrt{\mathcal{B}}, \quad (5.1)$$

corresponds to the situation where the particle size a is allowed to vary, while all other dimensional quantities are fixed. The second scenario,

$$\mathcal{S} \propto \mathcal{B}, \quad (5.2)$$

corresponds to the situation where it is the diffusivity D that is allowed to vary.

These linkages suggest that in an asymptotic analysis, we should study the situation where both numbers are either small or large. For small Damköhler numbers, the leading-order calculation is actually independent of the linkage. Indeed, it is evident from (3.3) that c is of order \mathcal{S} , while from (3.1) we see that at leading-order c is governed by Laplace's equation. Writing $c = \mathcal{S}\acute{c} + \dots$, we find from (3.3) that \acute{c} satisfies

$$\frac{\partial \acute{c}}{\partial r} = f(\theta) \quad \text{at} \quad r = 1. \quad (5.3)$$

Writing the harmonic field \acute{c} as a sum of spherical harmonics,

$$\acute{c} = \sum_{m=0}^{\infty} a_m \frac{P_m(\mu)}{r^{m+1}}, \quad (5.4)$$

we readily obtain using (3.9),

$$a_m = -(m + 1)^{-1} F_m \quad \text{for } m \neq 0. \quad (5.5)$$

The particle velocity is then obtained from (3.10), (3.12) and (5.5):

$$U = \frac{\mathcal{S}F_1}{3} + \dots. \quad (5.6)$$

This leading-order velocity is unaffected by bulk absorption.

VI. LARGE DAMKÖHLER NUMBERS

In the limit of large Damköhler numbers we find from (3.1) and (3.4) that

$$c \equiv 0. \quad (6.1)$$

Since this is an exact solution of both (3.1) and (3.4), it is evident the asymptotic error is exponentially small.

The trivial solution (6.1) is clearly incompatible with (3.3) at \mathcal{A} , the active portion of the boundary (see Fig. 1),

$$\mathcal{A} = \{\theta \in (0, \pi) | f(\theta) > 0\}. \quad (6.2)$$

Seeking an additional distinguished limit at large Damköhler numbers, we observe from (3.1) a possible dominant balance with spatial variations across a narrow region of $\text{ord}(\mathcal{B}^{-1/2})$ width. We therefore postulate a boundary layer of that width about \mathcal{A} . Defining the stretched coordinate

$$Y = \mathcal{B}^{1/2}(r - 1), \quad (6.3)$$

we write in the boundary layer

$$c(r, \theta; \mathcal{B}) = \tilde{c}(Y, \theta; \mathcal{B}). \quad (6.4)$$

Substitution of (6.3)–(6.4) into the diffusion–reaction equation (3.1) yields

$$\frac{\partial^2 \tilde{c}}{\partial Y^2} + \mathcal{B}^{-1/2} \frac{\partial \tilde{c}}{\partial Y} + \dots = \tilde{c} \quad \text{for } Y > 0. \quad (6.5)$$

Condition (3.3) becomes,

$$\mathcal{B}^{1/2} \frac{\partial \tilde{c}}{\partial Y} = \mathcal{S}(1 + \tilde{c})f(\theta) \quad \text{at } Y = 0, \quad (6.6)$$

and the requirement of matching with the “outer” solution (6.1) implies the far-field decay

$$\lim_{Y \rightarrow \infty} \tilde{c} = 0. \quad (6.7)$$

Once the boundary-layer problem is solved, the particle speed is readily obtained from (3.8) as

$$U = - \int_{\mathcal{A}} \tilde{c}|_{Y=0} \sin \theta \cos \theta d\theta. \quad (6.8)$$

We only seek the leading-order solution. Thus, we have from (6.5)

$$\frac{\partial^2 \tilde{c}}{\partial Y^2} = \tilde{c} \quad \text{for } Y > 0. \quad (6.9)$$

The solution of (6.7) and (6.9) is

$$\tilde{c}(Y, \theta) = -L(\theta)e^{-Y}. \quad (6.10)$$

Substitution into (6.8) gives

$$U = \int_{\mathcal{A}} L(\theta) \sin \theta \cos \theta d\theta. \quad (6.11)$$

Up to this point, the analysis has been independent of the linkage between \mathcal{B} and \mathcal{S} . The distribution $L(\theta)$, however, is determined by condition (6.6), whose leading-order form depends upon the specific linkage. The case (5.1) of linkage by size is conveniently represented by the relation

$$\mathcal{S} = \alpha \sqrt{\mathcal{B}}, \quad (6.12)$$

where α is fixed. Condition (6.6) then reads, at leading order,

$$\frac{\partial \tilde{c}}{\partial Y} = \alpha(1 + \tilde{c})f(\theta) \quad \text{at } Y = 0. \quad (6.13)$$

Substitution of (6.10) then gives

$$L(\theta) = \frac{\alpha f(\theta)}{1 + \alpha f(\theta)}. \quad (6.14)$$

We therefore find from (6.11) that, at leading order,

$$U = \alpha \int_{\mathcal{A}} \frac{f(\theta)}{1 + \alpha f(\theta)} \sin \theta \cos \theta d\theta. \quad (6.15)$$

The case (5.2) of linkage by diffusivity is represented by the relation,

$$\mathcal{S} = \beta \mathcal{B} \quad (6.16)$$

where β is considered fixed. Here, at leading order, condition (6.6) gives

$$\tilde{c} = -1 \quad \text{at} \quad Y = 0. \quad (6.17)$$

Substitution of (6.10) then gives

$$L(\theta) \equiv 1. \quad (6.18)$$

We therefore find from (6.11) that

$$U = \int_{\mathcal{A}} \sin \theta \cos \theta \, d\theta, \quad (6.19)$$

at leading order.

Remarkably, the particle velocity depends only upon the active fraction of boundary; it is independent of β and f and is accordingly insensitive to the details of the activity profile. In what follows, it is convenient to restrict the analysis to the case (see Fig. 1) where $\mathcal{A} = (0, \theta^*)$ with $0 < \theta^* < \pi$ [cf. (8.1) and (8.4)]. Under this modest restriction, (6.19) gives

$$U = \frac{\sin^2 \theta^*}{2}. \quad (6.20)$$

VII. TRANSITION REGION

The solution in the limit of large Damköhler numbers, with linkage by diffusivity, may appear to introduce a contradiction. Indeed, the nonzero velocity (6.20), which may be traced back to (3.8), is incompatible with the zero velocity predicted by a naive substitution of (6.10) and (6.18) into the original quadrature (3.7). The origin of this incompatibility has to do with smoothness at the boundary $r = 1$. Indeed, the excess concentration is discontinuous at the transition $\theta = \theta^*$ between \mathcal{A} , about which (6.10) and (6.18) hold, and its complement, about which (6.1) holds. With a finite discontinuity, expression (3.7) cannot be applied in a piecewise manner.

The resolution of this apparent contradiction has to do with a breakdown of the boundary-layer structure. The boundary-layer solution, where variations with respect to θ are assumed “small,” is clearly incompatible with a finite discontinuity. A transition region is therefore formed about the edge ($r = 1$ and $\theta = \theta^*$) of \mathcal{A} . In that region, the excess concentration smoothly varies from the boundary-layer solution (6.10) and (6.18) at $\theta < \theta^*$ to the nil value (6.1) at $\theta > \theta^*$. With the presence of such a region, the original quadrature (3.7) is

dominated by a small neighborhood \mathcal{N} of θ^* , which is still asymptotically larger than the width of the transition region. Since θ is approximately constant in that neighborhood, we obtain from (3.7)

$$U = \frac{\sin^2 \theta^*}{2} \int_{\mathcal{N}} \frac{\partial c}{\partial \theta} \Big|_{r=1} d\theta. \quad (7.1)$$

Recalling the need to match the minus unity value for $\theta^* > \theta$ and the zero value for $\theta > \theta^*$, we retrieve (6.20).

The boundary-layer scaling suggests that the lateral extent of the transition region is $\mathcal{B}^{-1/2}$. Defining the local coordinate [cf. (6.3)]

$$X = \mathcal{B}^{1/2}(\theta^* - \theta), \quad (7.2)$$

and considering the limit $\mathcal{B} \rightarrow \infty$ with X, Y fixed we find that the transition region coincides the upper half XY -plane (see Fig. 1). Defining $C(X, Y) = -c(r, \theta)$, C is governed by the modified Helmholtz equation

$$\frac{\partial^2 C}{\partial X^2} + \frac{\partial^2 C}{\partial Y^2} = C \quad \text{for } Y > 0. \quad (7.3)$$

At large Y it must satisfy

$$\lim_{Y \rightarrow \infty} C = 0, \quad (7.4)$$

representing asymptotic matching with (6.1).

It remains to specify the mixed boundary conditions at $Y = 0$, which follow from the exact condition (6.6) with linkage by diffusivity (6.16):

$$\frac{\partial C}{\partial Y} = -\beta \mathcal{B}^{1/2} (1 - C) f(\theta^* - \mathcal{B}^{-1/2} X) \quad \text{at } Y = 0. \quad (7.5)$$

In the inert portion of the boundary, where $f = 0$, we find

$$\frac{\partial C}{\partial Y} = 0 \quad \text{for } X < 0. \quad (7.6)$$

The condition on the active portion depends upon the asymptotic behavior of $f(\theta)$ as $\theta \nearrow \theta^*$. In the case where $f(\theta)$ attains there a nonzero limit [cf. (8.1)], applying the limit $\mathcal{B} \rightarrow \infty$ to (7.5) yields

$$C = 1 \quad \text{for } X > 0; \quad (7.7)$$

in the case where $f(\theta) \sim K(\theta^* - \theta)$ as $\theta \nearrow \theta^*$ [cf. (8.4), where $K = 1$], the appropriate condition in the limit $\mathcal{B} \rightarrow \infty$ is

$$\frac{\partial C}{\partial Y} = -\beta K (1 - C) X \quad \text{for } X > 0. \quad (7.8)$$

For situations where (7.7) holds, the problem is reminiscent of the diffraction of plane waves of sound by the edge of a semi-infinite screen — a problem originally solved by Sommerfeld [13]. Defining the local polar coordinates (ρ, ϑ) by

$$X = \rho \cos \vartheta, \quad Y = \rho \sin \vartheta \quad (7.9)$$

(see Fig. 1), the solution of (7.3)–(7.4) and (7.6)–(7.7), derived in the Appendix, is

$$C = \frac{e^{-Y}}{2} \left\{ 1 + \operatorname{erf} \left[\rho^{1/2} \left(\cos \frac{\vartheta}{2} - \sin \frac{\vartheta}{2} \right) \right] \right\} + \frac{e^Y}{2} \left\{ 1 - \operatorname{erf} \left[\rho^{1/2} \left(\cos \frac{\vartheta}{2} + \sin \frac{\vartheta}{2} \right) \right] \right\}. \quad (7.10)$$

In terms of the polar coordinates (7.9), the limit $X \rightarrow \infty$ with Y fixed corresponds to $\rho \rightarrow \infty$ with $\vartheta = O(1/\rho)$. We then readily obtain

$$\lim_{X \rightarrow \infty} C = e^{-Y}, \quad (7.11)$$

which trivially matches the boundary-layer solution (6.10) and (6.18). The limit $X \rightarrow -\infty$ with Y fixed corresponds to $\rho \rightarrow \infty$ with $\pi - \vartheta = O(1/\rho)$. Here, we obtain

$$\lim_{X \rightarrow -\infty} C = 0, \quad (7.12)$$

which trivially matches the nil concentration about the inert portion of the particle boundary.

VIII. ILLUSTRATIONS

We continue by illustrating our results, considering first the case of linkage by size. With \mathcal{B} locked to \mathcal{S} via (6.12), U becomes a function of \mathcal{S} , α and the activity profile. We use a Janus configuration, namely

$$f(\theta) = \begin{cases} 1, & 0 < \theta < \pi/2, \\ 0, & \pi/2 < \theta < \pi, \end{cases} \quad (8.1)$$

for which (3.11) gives

$$F_{2k} = \frac{\delta_{k,0}}{2}, \quad F_{2k+1} = \frac{(-)^k (2k)! (4k+3)}{2^{2k+2} (k!)^2 (k+1)}, \quad (8.2)$$

and, in particular, $F_1 = 3/4$. The velocity calculated using (4.3) is shown in Fig. 2 for $\alpha = 1/2, 1$ and 2 . We also portray the α -independent small Damköhler-number approximation

(5.6), which here gives $U = \mathcal{S}/4$ for $\mathcal{S} \ll 1$. With (8.1), the large Damköhler-number approximation (6.15) gives

$$\lim_{\mathcal{S} \rightarrow \infty} U = \frac{\alpha}{2(1 + \alpha)}. \quad (8.3)$$

For the aforementioned α values, it implies the respective limits 1/6, 1/4 and 1/3. The approach at large \mathcal{S} to these limits is evident in the figure.

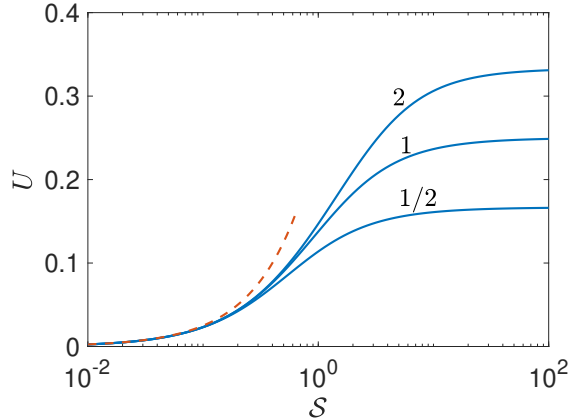


FIG. 2. U versus \mathcal{S} using linkage-by-size (6.12) for the Janus profile (8.1). Solid: exact result (4.3) for the indicated values of α . Dashed: small- \mathcal{S} approximation (5.6).

Consider now the linkage by diffusivity. With \mathcal{B} locked to \mathcal{S} via (6.16), U becomes a function of \mathcal{S} , β and the activity profile. We here use a single linkage value, $\beta = 1$, but consider both the Janus activity distribution (8.1) and the generalized Janus profile

$$f(\theta) = \begin{cases} \cos \theta, & 0 < \theta < \pi/2, \\ 0, & \pi/2 < \theta < \pi, \end{cases} \quad (8.4)$$

for which

$$F_{2k} = \frac{(-)^{k+1}(2k)!(4k+1)}{4^{k+1}(k!)^2(k+1)(2k-1)}, \quad F_{2k+1} = \frac{\delta_{k0}}{2}, \quad (8.5)$$

and, in particular, $F_1 = 1/2$. For that profile the small Damköhler-number approximation (5.6) gives $U = \mathcal{S}/6$ for $\mathcal{S} \ll 1$. Since $\mathcal{A} = (0, \pi/2)$ for both (8.1) and (8.4), these distributions share the same large Damköhler-number limit (6.20), namely

$$\lim_{\mathcal{S} \rightarrow \infty} U = \frac{1}{2}. \quad (8.6)$$

The results are illustrated in Fig. (3).

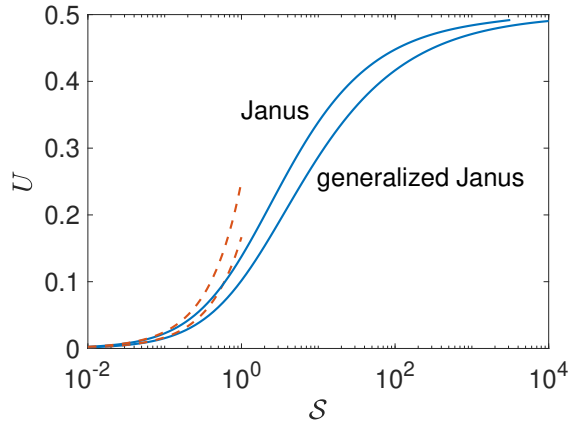


FIG. 3. U versus \mathcal{B} using linkage-by-diffusivity (6.16) with $\beta = 1$ for both the Janus (8.1) and the generalized Janus (8.4) activity profiles. Solid: exact result (4.3). Dashed: small Damköhler-number approximation (5.6).

In calculating U using (4.3), we have encountered difficulties when applying the numerical scheme at large values of \mathcal{S} . These are more pronounced for the Janus profile (8.1), where the interfacial activity undergoes a finite discontinuity at $\theta = \pi/2$. Apparently, the associated non-smoothness escalates the Gibbs phenomenon. In any event, the approach to the limit (8.6) is unequivocal.

IX. CONCLUDING REMARKS

We have analyzed self-phoresis of active colloids in situations where solute is transported by diffusion and consumed by two chemical reactions, one at the colloid boundary and one within the bulk. The dimensionless problem is governed by the two associated Damköhler numbers, \mathcal{S} and \mathcal{B} .

We have solved the problem using an eigenfunction expansion. This semi-analytic solution, applicable for all values of \mathcal{S} and \mathcal{B} , has been accompanied by asymptotic approximations. The chosen limits correspond to two possible natural linkages between \mathcal{S} and \mathcal{B} . For small Damköhler numbers, the particle velocity is proportional to \mathcal{S} and independent of \mathcal{B} . At large Damköhler numbers, the solute concentration is uniform except within a boundary layer about the active portion of the boundary. The details of the boundary-layer transport depend upon the linkage between \mathcal{S} and \mathcal{B} . In particular, for $\mathcal{S} \propto \mathcal{B}$ we find that the particle

velocity depends upon the relative fraction of the active boundary, but is otherwise indifferent to the activity details in that fraction. The associated boundary-layer solution breaks down near the edge of the active portion of the boundary. Following a similar analysis in a classical wave problem [13], we have obtained a close-form solution of the local transport problem in the edge region.

We summarize our results in terms of dimensional quantities. For weak chemical activity, the particle velocity is proportional to $b\bar{k}c_\infty/D$. This size-independent scaling is the same as in the simplest models of flux-prescribed distributions [2], the flux scale being $\bar{k}c_\infty$. In the limit of strong activity, the velocity scales as bc_∞/a . Here, there are two situations. If the limit is realized by large values of a , the ratio of the particle velocity to bc_∞/a depends (nonlinearly) upon both the ratio $\alpha = \bar{k}/\sqrt{k_b D}$ and the activity profile. If the limit is realized by small values of D , the ratio of the particle velocity to bc_∞/a is independent of the reaction coefficients, the solute diffusivity, and even the details of the reaction profile.

Appendix: Transition region

Following [14], we seek a solution of (7.3) of the form

$$C = e^{-Y}G + e^Y H. \quad (\text{A.1})$$

Requiring the functions G and H to satisfy

$$\frac{\partial^2 G}{\partial X^2} + \frac{\partial^2 G}{\partial Y^2} = 2\frac{\partial G}{\partial Y}, \quad \frac{\partial^2 H}{\partial X^2} + \frac{\partial^2 H}{\partial Y^2} = -2\frac{\partial H}{\partial Y}, \quad (\text{A.2})$$

(7.3) is trivially satisfied. To solve equations (A.2), we employ the parabolic-cylinder coordinates (see Fig. 1)

$$\xi = \rho^{1/2} \cos \frac{\vartheta}{2}, \quad \eta = \rho^{1/2} \sin \frac{\vartheta}{2}. \quad (\text{A.3})$$

These are natural for the transition-region geometry and conditions (7.6)–(7.7), since the negative real axis becomes $\xi = 0$, while the positive real axis becomes $\eta = 0$. With ξ and η as independent variables, (A.2) become

$$\frac{\partial^2 G}{\partial \xi^2} + \frac{\partial^2 G}{\partial \eta^2} = 4 \left(\eta \frac{\partial G}{\partial \xi} + \xi \frac{\partial G}{\partial \eta} \right), \quad \frac{\partial^2 H}{\partial \xi^2} + \frac{\partial^2 H}{\partial \eta^2} = -4 \left(\eta \frac{\partial H}{\partial \xi} + \xi \frac{\partial H}{\partial \eta} \right). \quad (\text{A.4a, b})$$

The solution to (A.4a) can be written as a combination of two similarity solutions,

$$G = G_+(\zeta_+) + G_-(\zeta_-), \quad (\text{A.5})$$

wherein $\zeta_{\pm} = \xi \pm \eta$. We therefore obtain the ordinary differential equations,

$$G''_+ = 2\zeta_+ G'_+, \quad G''_- = -2\zeta_- G'_-, \quad (\text{A.6})$$

which integrate to give $G'_{\pm} = g_{\pm} e^{\pm\zeta_{\pm}^2}$. Similarly, the solution to (A.4b) is written as a combination of two similarity solutions,

$$H = H_+(\zeta_+) + H_-(\zeta_-). \quad (\text{A.7})$$

The resulting equations,

$$H''_+ = -2\zeta_+ H'_+, \quad H''_- = 2\zeta_- H'_-, \quad (\text{A.8})$$

integrate to give $H'_{\pm} = h_{\pm} e^{\mp\zeta_{\pm}^2}$.

Now, as $\rho \rightarrow \infty$, it is evident that $\zeta_+ \rightarrow \infty$ for all $0 < \vartheta < \pi$ while ζ_- tends to ∞ for $0 < \vartheta < \pi/2$ and to $-\infty$ for $\pi/2 < \vartheta < \pi$. To avoid a super-exponential divergence of C at large ρ , which would clearly contradict (7.4), we must set $g_+ = h_- = 0$. We conclude that the most general solutions of (A.4) are

$$G(\xi, \eta) = \dot{g} + g \operatorname{erf}(\xi - \eta), \quad H(\xi, \eta) = \dot{h} + h \operatorname{erf}(\xi + \eta). \quad (\text{A.9})$$

The four constants appearing in (A.9) are determined from the boundary conditions. With condition (7.6) applying at $\xi = 0$ we readily obtain $\dot{h} = \dot{g}$ and $h = -g$. Thus, (A.1) and (A.9) give

$$C = e^{-Y} [\dot{g} + g \operatorname{erf}(\xi - \eta)] + e^Y [\dot{g} - g \operatorname{erf}(\xi + \eta)]. \quad (\text{A.10})$$

Recalling that $\operatorname{erf} z \sim 1 - e^{-z^2}/z\sqrt{\pi}$ for $z \rightarrow \infty$, we must impose $\dot{g} = g$ to satisfy condition (7.4). Last, noting that the inhomogeneous condition (7.7) applies at $\eta = 0$, we readily obtain $g = 1/2$. We conclude that

$$C = \frac{e^{-Y}}{2} [1 + \operatorname{erf}(\xi - \eta)] + \frac{e^Y}{2} [1 - \operatorname{erf}(\xi + \eta)]. \quad (\text{A.11})$$

Substitution of (A.3) yields (7.10).

-
- [1] A. Aubret, S. Ramanarivo, and J. Palacci, Eppur si muove, and yet it moves: Patchy (phoretic) swimmers, *Curr. Opin. Colloid Interface Sci.* **30**, 1 (2017).
- [2] R. Golestanian, T. B. Liverpool, and A. Ajdari, Designing phoretic micro-and nano-swimmers, *New J. Phys.* **9**, 126 (2007).

- [3] J. L. Anderson, Colloid transport by interfacial forces, *Annu. Rev. Fluid Mech.* **30**, 139 (1989).
- [4] S. Ebbens, M.-H. Tu, J. R. Howse, and R. Golestanian, Size dependence of the propulsion velocity for catalytic Janus-sphere swimmers, *Phys. Rev. E* **85**, 020401 (2012).
- [5] P. De Buyl, A. S. Mikhailov, and R. Kapral, Self-propulsion through symmetry breaking, *Europhy. Lett.* **103**, 60009 (2013).
- [6] O. Schnitzer, Weakly nonlinear dynamics of a chemically active particle near the threshold for spontaneous motion. I. Adjoint method, *Phys. Rev. Fluids* **8**, 034201 (2023).
- [7] D. Sondak, C. Hawley, S. Heng, R. Vinsonhaler, E. Lauga, and J.-L. Thiffeault, Can phoretic particles swim in two dimensions?, *Phys. Rev. E* **94**, 062606 (2016).
- [8] E. Yariv, Two-dimensional phoretic swimmers: the singular weak-advection limits, *J. Fluid Mech.* **816**, R3 (2017).
- [9] F. Picella and S. Michelin, Confined self-propulsion of an isotropic active colloid, *J. Fluid Mech.* **933**, A27 (2022).
- [10] N. Yoshinaga, K. H. Nagai, Y. Sumino, and H. Kitahata, Drift instability in the motion of a fluid droplet with a chemically reactive surface driven by Marangoni flow, *Phys. Rev. E* **86**, 016108 (2012), 1206.3625.
- [11] S. Michelin and E. Lauga, Phoretic self-propulsion at finite Péclet numbers, *J. Fluid Mech.* **747**, 572 (2014).
- [12] H. A. Stone and A. D. T. Samuel, Propulsion of microorganisms by surface distortions, *Phys. Rev. Lett.* **77**, 4102 (1996).
- [13] A. Sommerfeld, Mathematische theorie der diffraktion: Mit einer tafel, *Math. Ann.* **47**, 317 (1896).
- [14] H. Lamb, On Sommerfeld's diffraction problem, and on reflection by a parabolic mirror, *Proceedings of the London Mathematical Society* **2**, 190 (1907).